CrossMark

Regulation and control of insulated layers for intergranular insulated Fe/SiO$_2$ soft magnetic composites

Jian Wang[1,2,3], Xi'an Fan[1,2,5,*], Zhaoyang Wu[1,2,4,5], and Guangqiang Li[1,2,5]

[1] *The State Key Laboratory of Refractories and Metallurgy, Wuhan University of Science and Technology, Wuhan 430081, Hubei, People's Republic of China*

[2] *Key Laboratory for Ferrous Metallurgy and Resources Utilization of Ministry of Education, Wuhan University of Science and Technology, Wuhan 430081, Hubei, People's Republic of China*

[3] *Guangdong Institute of Materials and Processing, Guangdong Academy of Sciences, 363 Changxing Rd., Tianhe District, Guangzhou 510650, Guangdong, People's Republic of China*

[4] *School of Metallurgical Engineering, Anhui University of Technology, Maanshan 243002, Anhui, People's Republic of China*

[5] *School of Materials and Metallurgy, Wuhan University of Science and Technology, 185#, 947 Heping Road, Qingshan District, Wuhan 430081, People's Republic of China*

ABSTRACT

In this work, the intergranular insulated Fe/SiO$_2$ soft magnetic composite cores with tunable insulating layer thickness were prepared by a modified Stöber method combined with the spark plasma sintering technology. Most of the conductive Fe particles could be coated uniformly by insulated SiO$_2$ using the modified Stöber method, and the high compact and intergranular insulated cores could be obtained quickly by the spark plasma sintering process. The intergranular insulated Fe/SiO$_2$ composite cores exhibited much higher electrical resistivity, lower core loss, better frequency stability of permeability and large higher quality factor than that of raw Fe core without insulated SiO$_2$. The thickness of SiO$_2$ insulating layer, electrical and magnetic properties of intergranular insulated Fe/SiO$_2$ composite cores could be readily controlled by adjusting the tetraethyl orthosilicate concentration. The thickness of SiO$_2$ insulating layer and resistivity of Fe/SiO$_2$ composite cores first increased and then dropped with increasing the tetraethyl orthosilicate concentration, while the permeability and core loss changed in the opposite direction. Fe/SiO2 composite core showed the optimal performance when the tetraethyl orthosilicate concentration was 0.135 mol l^{-1}, which exhibited better frequency stability at high frequencies, much higher electrical resistivity, higher quality factor and lower core loss.

Address correspondence to E-mail: groupfxa@163.com; xafan@wust.edu.cn

Springer

Introduction

Thanks to the development of powder metallurgy, the soft magnetic composites (SMCs) have been employed widely to design the magnetic cores for various AC and DC electromagnetic applications [1]. Consisting of ferromagnetic powder particles coated with electrical insulating layer, the SMCs offer some unique properties such as high electrical resistivity, 3D isotropic ferromagnetic behavior, good relative permeability, very low eddy current loss and relatively low total core loss at medium and high frequencies [2–6]. Nowadays the demand for efficient generation, transmission and distribution of electric power is ever growing, while the annual electric losses are surpassing annual increases in electricity consumption [7]. As the key materials of electromagnetic transduction, there is an ever-increasing need for SMCs with better soft magnetic properties and their core losses are the most important parameters for applications.

Generally, the SMCs are produced by powder metallurgy process including mixing soft ferromagnetic powder particles with insulating phases and lubricant substances, compacting and pressing them to the desired shape, as well as a subsequent annealing treatment for relieving stress [8]. To prepare high-performance SMCs with lower core losses and optimum magnetic properties, it is very important to select suitable coating materials and coating process. Thus, many efforts have been carried out to improve the magnetic performance of the SMCs by selecting suitable inorganic or/and organic insulating material and applying suitable coating method. Resin as the most common organic coating agent has been used to bond and cover magnetic particles in SMCs [9–12]. But the stress relief of the SMCs with organic coating cannot be completed as the thermal treatment temperature is limited to below 500 °C, which results in higher coercivity and hysteresis loss [13, 14]. Therefore, some inorganic materials (SiO_2, CuO, MgO, Fe_2O_3, Al_2O_3, etc.) were used as the insulating layers [15–22] to prepare SMCs. FeSiAl SMCs with hybrid phosphate–alumina coating presented significantly improved soft magnetic performance [16]. FeSiAl-based soft magnetic composites with Al_2O_3 and AlN insulating coating can obviously increase electrical resistivity, decrease the loss factor and improve the frequency stability and the quality factor in high-frequency range [17].

As it is well known, as the insulated layer, the inorganic materials are nonmagnetic and their presence will degrade the magnetic induction. Thus, it is critical to control the amount and thickness of insulating coating inside SMCs to obtain the balance between the low core loss and high magnetic induction. In the following work, we tried to control the thickness of insulating layer and investigated the effect of the thickness of insulating layer on the electrical and magnetic properties of Fe/SiO_2 soft magnetic composites to obtain the balance between the low core loss and high magnetic induction. In order to achieve the above objects, silica as the coating agent was used to prepare Fe/SiO_2 core–shell particles by a modified Stöber process with a silane-coupling agent as modification additives [23, 24] and various amounts of tetraethyl orthosilicate were used to provide the silicon source to produce Fe/SiO_2 core–shell particles with different thickness of the coating layer. And then the subsequently spark plasma sintering (SPS) technology was used to consolidate the composite cores. The magnetic powder particles are separated by SiO_2 layer, which can prevent the eddy current paths; the eddy current is confined within the magnetic powder particles and hence reduces the eddy current losses induced by AC magnetic field.

Experimental

The raw material is spherical/quasi-spherical carbonyl iron powder with an average particle size of <10 μm. 3-Triethoxysilypropylamine (APTES, 99 wt%), tetraethyl orthosilicate (TEOS, 98 wt%+), aqueous ammonia (28 wt%, lab grade) and absolute ethanol were purchased from Tianli Chemical Reagent Company, Tianjin, China. Distilled water (H_2O) was obtained by Automatic Double Pure Water Distillatory (SZ-93A, China) in laboratory. All chemicals used were of analytical grade and were used as received without further purification.

In a typical chemical coating procedure, 50 g carbonyl iron powder particles, 3.0 g APTES and 10 ml deionized water were dispersed in 500 ml absolute ethanol by mechanical stirring for 1 h at 50 °C. Then, the reaction temperature was raised to 60 °C and 2 ml aqueous ammonia (25 wt%) and a certain concentration of TEOS was introduced by dripping slowly using injection pump (LSP01-1A) at a constant speed for 20 h. After washing with absolute ethanol
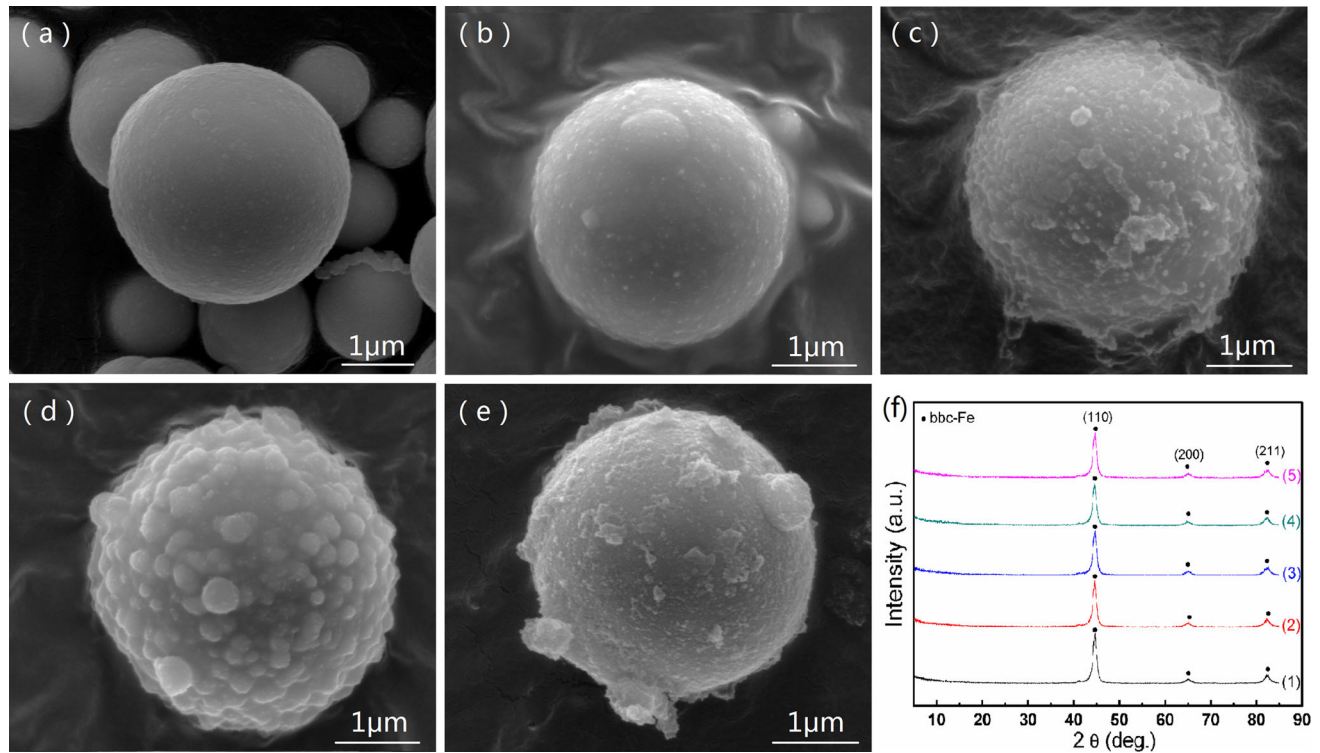
Figure 1 SEM images of Fe particles before (**a**) and after chemical coating process added TEOS concentration of 0.045 mol l^{-1} (**b**), 0.090 mol l^{-1} (**c**), 0.135 mol l^{-1} (**d**) and 0.180 mol l^{-1} (**e**); **f** XRD patterns of Fe particles before (*1*) and after chemical coating process added TEOS concentration of 0.045 mol l^{-1} (*2*), 0.090 mol l^{-1} (*3*), 0.135 mol l^{-1} (*4*) and 0.180 mol l^{-1} (*5*).

several times, the suspension was dried at 60 °C for 24 h. During the chemical coating process, various concentrations of TEOS ranging from 0.045 to 0.180 mol l^{-1} were used to produce Fe/SiO$_2$ core–shell particles. The Fe/SiO$_2$ core–shell particles obtained above were sintered at 1050 °C under a uniaxial pressure of 30 MPa by SPS process with a heating rate of 50 °C·min^{-1}. In all the cases, the holding time at the sintering temperature was 10 min. Finally, the Fe/SiO$_2$ composite cores (outer diameter = 20.3 mm, inner diameter = 12.7 mm, height = 6.35 mm) were obtained after annealing at 800 °C for 2 h under pure argon atmosphere to release the internal stress. To investigate the effect of insulated SiO$_2$ layer on the electrical and magnetic properties, the raw Fe core without insulated SiO$_2$ layer was also prepared under the same conditions.

X-ray diffraction (XRD) was analyzed on an X-Pert Philips diffractometer with Cu Kα radiation (λ = 1.5418 Å). The morphology and local chemical homogeneity of the as-prepared samples were observed by scanning electron microscopy (SEM) (Nova 400) equipped with an energy-dispersive X-

ray spectrometer (EDS) (IE350PentaFETX-3). Fourier transform infrared spectra (FTIR) were recorded in the wave number range from 400 to 4000 cm^{-1} at room temperature. The real density of raw Fe particles and Fe/SiO$_2$ core–shell particles was measured using an automatic density analyzer (AccuPyc 1330). The resistivity was measured by a four-probe method. Core loss at high frequency was obtained by an autotesting system for magnetic materials (MATS-2010SA). The inductance (*L*) and quality factor (*Q*) were measured under a constant voltage of 0.3 V in a frequency range from 50 Hz to 1000 kHz by impedance analyzer (HIOKI 3532-50 LCR HiTESTER). The effective permeability (μ_{eff}) was calculated using the following formula (1) [25, 26]:

$$\mu_{eff} = \frac{\bar{l}L}{\mu_0 N^2 A} \tag{1}$$

where $\bar{l}$ means the average length of the magnetic circuit, *N* refers to the number of turns of inductor, *A* stands for the effective area of magnetic circuit, μ_0 represents the permeability of vacuum, and it is $4\pi \times 10^{-7}$ H m^{-1}.

Results and discussion

Figure 1a–e shows the SEM images of Fe particles before and after chemical coating process added different TEOS concentration. All of the particle samples are micron-grade spheroids with a diameter of less than 10 μm. It can be seen that the surface of raw Fe particles is very smooth and clean (Fig. 1a). When introducing TEOS concentration of 0.045 mol l^{-1}, the surface of Fe particles became rough as shown in Fig. 1b. With TEOS concentration increased to 0.090 mol l^{-1}, the surface tended to be rougher and coated with some deposition gathered with nanoscaled particles (Fig. 1c). The size and quantity of nanoparticles were increased obviously with increasing the TEOS concentration. When the TEOS concentration is increased to 0.135 mol l^{-1}, the Fe particles were completely covered with a layer of nanoparticles (Fig. 1d). With further increasing the TEOS concentration to 0.180 mol l^{-1}, some free
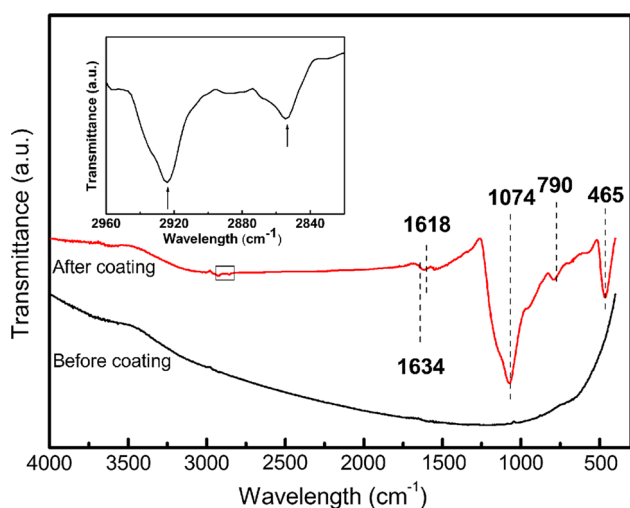

Figure 2 FTIR spectra of the Fe particles before and after chemical coating process.

flocculent precipitate formed and most of them aggregated away from the Fe particles (Fig. 1e).

Figure 1f shows the corresponding XRD patterns of Fe particles before and after chemical coating process added different TEOS concentration. The three distinguishable diffraction peaks at 2θ of 44.663° (110), 65.008° (200) and 82.314° (211) of crystalline iron with body-centered cubic (BBC) structure [space group *Im-3m* (229), JCPDS 03-065-4899] can be detected in all particle samples. The other diffraction peaks are absent even for Fe particle samples added TEOS concentration of 0.135 mol l^{-1}, suggesting that the obtained coating layer may be amorphous.

The chemical compositions of Fe particles after chemical coating process added different TEOS concentration are characterized by EDS as depicted in Table 1. As revealed in Table 1, only elements Fe and O exist on the surface of raw Fe particles, but another Si signal is also present after chemical coating. And the concentration of Si and O elements increases from 0 and 2.74 wt% to 9.35 and 12.99 wt % with increasing TEOS concentration from 0.045 to 0.135 mol l^{-1}, respectively, causing the opposite tendencies for Fe element. However, with further increasing TEOS concentration to 0.180 mol l^{-1}, the concentrations of Si and O elements declined to 3.02 and 8.74 wt %, respectively. It is because the free flocculent precipitate containing Si and O elements was formed away Fe particles instead of coating on their surface. It is evident that the obtained coating containing Si and O elements should be SiO$_2$. Concentration variations of Si and O elements should be attributed to the changes of thickness for SiO$_2$ coating layer.

To gain further insight into the microstructure of the coating layer coated on Fe particles, the FTIR measurements were taken for both of Fe particles before and after chemical coating process (Fig. 2). By comparing their spectra, it can be found that there is

Table 1 EDS analysis of raw Fe particles and Fe particles after chemical coating process added different TEOS concentration

TEOS concentration (mol l^{-1})	Elements (wt %)			
	Fe K	O K	Si K	Totals
Raw Fe particles				
	97.26	2.74	–	100
Fe particles after coating				
0.045	92.95	4.5	2.55	100
0.090	85.45	6.09	8.46	100
0.135	77.66	12.99	9.35	100
0.180	88.24	8.74	3.02	100

Table 2 The densities of raw Fe particles and Fe particles after chemical coating process added different TEOS concentration

Density	Raw Fe particles	Fe particles after coating			
		0.045 mol l^{-1}	0.090 mol l^{-1}	0.135 mol l^{-1}	0.180 mol l^{-1}
ρ (g cm^{-3})	7.78	7.63	6.51	5.75	5.85
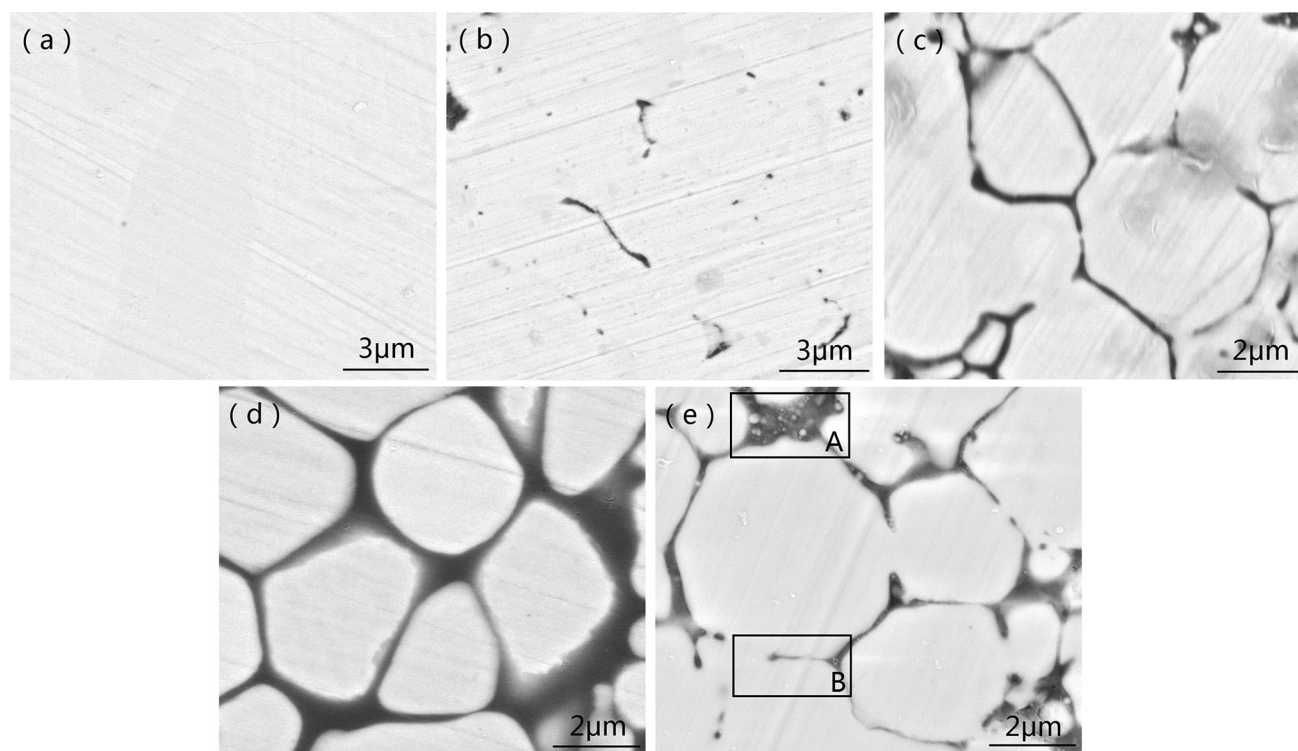
Figure 3 SEM image (*backscatter images*) of the polished surface for the sintered samples from raw Fe particles (**a**) and Fe/SiO$_2$ core–shell particles added TEOS concentration of 0.045 mol l^{-1} (**b**), 0.090 mol l^{-1} (**c**), 0.135 mol l^{-1} (**d**) and 0.180 mol l^{-1} (**e**).

no characteristic absorption peak for raw Fe particles, while some strong absorption peaks occur after chemical coating. The peak of 1634 cm^{-1} is attributed to the adsorbed water and structural hydroxyl groups, which is the characteristic of the bending vibration of δ(H–O–H) [27, 28]. Two weak absorption peaks near 2900 cm^{-1} are owing to the symmetric and asymmetric vibration of C–H bands originated from C$_2$H$_5$OH [29]. And the strongest band centered at 1074, 790 and 465 cm^{-1} corresponds to the asymmetric stretching of Si–O–Si, the symmetric stretching of Si–O–Si and the bending of O–Si–O, respectively [30, 31]. The result of FTIR confirms that the obtained coating layers on the surface of Fe particles are SiO$_2$.

Table 2 illustrates the evolution of the densities of raw Fe particles and Fe particles after chemical coating process. Fe particles after chemical coating show lower densities than that of raw Fe particles

(7.78 g cm^{-3}) without SiO$_2$ coated on their surface. And the densities of the composite powders drop from 7.63 to 5.75 g cm^{-3} with increasing the TEOS concentration from 0.045 to 0.135 mol l^{-1}, while rise up to 5.85 g cm^{-3} with further increasing TEOS concentration to 0.180 mol l^{-1}, which should be ascribed to the decreasing coating thickness of the amorphous SiO$_2$ layer due to their dissociation and aggregation.

Analyses above demonstrate that the layer coated on Fe particles must be amorphous SiO$_2$ and the Fe/SiO$_2$ core–shell particles are obtained successfully. The thickness of amorphous SiO$_2$ layer can be adjusted and controlled by varying the TEOS concentration. With increasing TEOS concentration from 0.045 to 0.180 mol l^{-1}, the thickness of SiO$_2$ layer first increases and then drops. High concentration of TEOS leads to a fast hydrolysis rate, the monomer
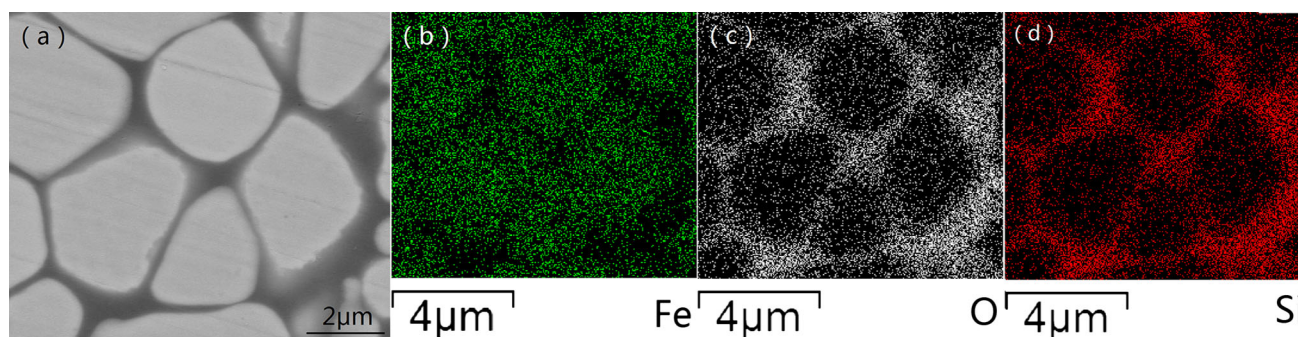
Figure 4 SEM micrograph for cross sections of Fe/SiO$_2$ composite core with TEOS concentration of 0.135 mol l^{-1} and corresponding elements distribution mapping (**a**), Fe (**b**), O (**c**) and Si (**d**).

Table 3 Comparison of electrical resistivity and core loss between the raw Fe core and Fe/SiO$_2$ composite cores

TEOS concentration (mol l^{-1})	ρ ($\mu\Omega$ m)	Core loss (W kg^{-1}): $P_{10 \text{ mT}/x \text{ KHz}}$					
		x = 10	x = 30	x = 50	x = 70	x = 110	x = 130
Raw Fe core							
0	0.13	12.44	59.24	120.20	190.81	310.80	448.54
Fe/SiO$_2$ composite core							
0.045	0.147	10.59	49.34	103.1	167.3	275.2	405
0.090	0.498	9.954	48.94	99	161.4	262.9	383.1
0.135	8.53	3.139	23.07	57.47	103.29	187.78	283.76
0.180	0.689	8.875	43.28	87.59	140.3	231.5	337.12

and oligomer of polysiloxane agglomerated before coating on the surface of Fe particles. When introducing TEOS of 0.135 mol l^{-1}, the Fe/SiO$_2$ core–shell particles show the maximum coating thickness.

Figure 3 shows the SEM images of the polished surfaces for the sintered samples from raw Fe particles (raw Fe core) and Fe/SiO$_2$ core–shell particles added different TEOS concentration (Fe/SiO$_2$ composite cores). From the cross section of all cores, we can see that the structure is compacting and no significant defect is observed. For raw Fe core (Fig. 3a), only gray-white zones distribute on the polished surface, while another gray-black zone is found for the Fe/SiO$_2$ composite cores. With increasing TEOS concentration from 0.045 to 0.135 mol l^{-1}, the amounts or thicknesses of gray-black zones increase clearly. In particular, for Fe/SiO$_2$ composite core prepared by introducing TEOS of 0.135 mol l^{-1}, gray-white zones are separated by gray-black zones or the gray-white zones are enclosed by gray-black zones completely. While with further increasing TEOS concentration to 0.180 mol l^{-1}, the nonuniform distribution of gray-black zones is occurred, such as

regions A and B in Fig. 3e, and the amount or thickness of gray-black zones decreases. This should be attributed to the formation of free flocculent precipitate.

The EDS analysis of Fe/SiO$_2$ composite core introduced TEOS of 0.135 mol l^{-1} is shown in Fig. 4. The EDS analysis reveals that element Fe distributes mainly in the gray-white zones and elements Si, O distribute mainly in gray-black zones. Namely, Fe particles are surrounded by SiO$_2$. The element Fe distributes at the core zones and SiO$_2$ distributes around the core particles, or it can be stated that the Fe particles are isolated from each other by SiO$_2$ layer.

Based on these observations, the intergranular insulated Fe/SiO$_2$ composite cores have been obtained. The thickness of insulated SiO$_2$ layer increased with increasing the TEOS concentration from 0.045 to 0.135 mol l^{-1}. And with further increasing the TEOS concentration to 0.180 mol l^{-1}, the thickness of insulated SiO$_2$ layer decreased because the free SiO$_2$ agglomerates together instead of coating on the surface of Fe particles.

Table 3 shows the total core loss as a function of frequency for raw Fe core and Fe/SiO$_2$ composite cores measured under magnetic field of 10 mT. The electrical resistivities are also summarized in Table 3. All Fe/SiO$_2$ composite cores exhibit higher electrical resistivity than that of raw Fe core due to the presence of insulated SiO$_2$ layers between Fe particles. The resistivity of Fe/SiO$_2$ composite core first increases and then decreases with increasing the TEOS concentration. When introducing TEOS of 0.135 mol l^{-1}, the Fe/SiO$_2$ composite core shows the maximum resistivity of 8.53 μΩ m.

In addition, the increasing core loss is observed for all the cores with raising testing frequency. Under the same testing conditions, Fe/SiO$_2$ composite cores show much lower core loss than raw Fe core because of the existence of insulated SiO$_2$ between Fe particles. The total core loss of SMCs in AC applications can be expressed as [30]:

$$W \approx W_e + W_h = \frac{CB^2f^2d^2}{\rho} + f \oint H \, \mathrm{d}B \quad (2)$$

where C means constant, ρ stands for the resistivity, B refers to the magnetic flux density, f represents the frequency, and d is the thickness of bulk materials. The insulated SiO$_2$ layer not only can increase the ρ but also can confine the eddy current in individual Fe particles to reduce the effective radius of eddy current at the same time, resulting in lower core loss. It is also noticed that the core loss of Fe/SiO$_2$ composite core changed with opposite tendency compared with the resistivity with increasing the TEOS concentration, which should be ascribed to the thickness and uniformity of the insulated SiO$_2$ layer. When introducing 0.045 mol l^{-1} TEOS, there are only a very small amount of SiO$_2$ distributed between Fe particle and the insulation effect is poor, so resulting in low resistivity and high core loss. When the TEOS concentration was 0.135 mol l^{-1}, the thickness and uniformity of the insulated SiO$_2$ layer is optimal and Fe/SiO$_2$ composite core present with the highest resistivity and lowest core loss due to most of eddy current is confined in the Fe particles. The $P_{10 \text{ mT}/10 \text{ kHz}}$ of Fe/SiO$_2$ composite core added TEOS of 0.135 mol l^{-1} (3.14 W kg^{-1}) is only about a quarter of that of the raw Fe core (12.44 W kg^{-1}). Unfortunately, when the TEOS concentration was further increased to 0.180 mol l^{-1}, the thickness and uniformity of the insulated SiO$_2$ layer between Fe particles decreases due to the dissociation and aggregation of
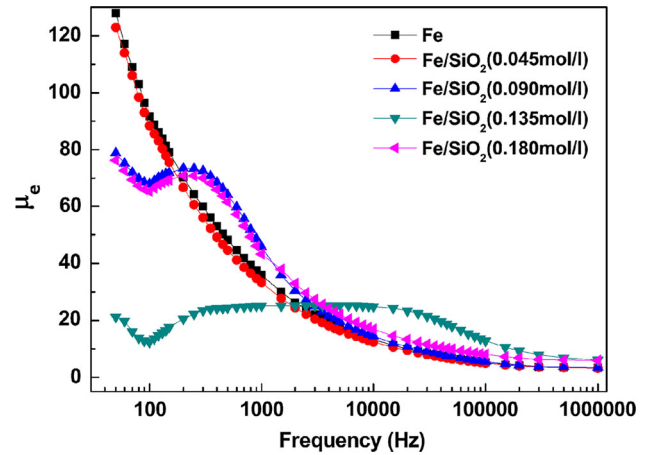

Figure 5 Effective permeability as a function of frequency for the raw Fe core and Fe/SiO$_2$ composite cores added different TEOS concentration.

SiO$_2$, resulting in the abnormal low resistivity and high core loss.

Figure 5 depicts the variation of μ_{eff} with frequency for raw Fe core and Fe/SiO$_2$ composite cores added different TEOS concentration. The value of μ_{eff} for most samples firstly drops intensely with testing frequency and then becomes stable, which is connected with the variation of L with frequency. The L was measured to characterize the μ_{eff} by means of conversion of formula (1). At high frequencies, the effective resistance of the conductor increases because of the skin effect phenomenon, thus decreasing the skin depth and effective cross section of the conductor. Less effective cross section of the conductor means less L. The value of L is inversely proportional to frequency, so is μ_{eff}. At low frequencies (<2 kHz), the value of μ_{eff} for Fe/SiO$_2$ composite core is much lower than that of raw Fe core due to the introduction of nonmagnetic SiO$_2$ phases. What's more, acting as an air gap, insulated SiO$_2$ layers generate more inner demagnetizing field, resulting in a smaller μ_{eff} [31]. Interestingly, Fe/SiO$_2$ composite cores exhibit better frequency stability at the high frequencies (>2 kHz) due to the decreasing eddy current. Smaller eddy current leads to larger skin depth and advanced frequency stability [32]. For Fe/SiO$_2$ composite cores, frequency stability of μ_{eff} tends to be better with increasing TEOS concentration from 0.045 to 0.135 mol l^{-1}, but it falls with further increasing TEOS concentration to 0.180 mol l^{-1}, which is closely linked with the variation of eddy current.
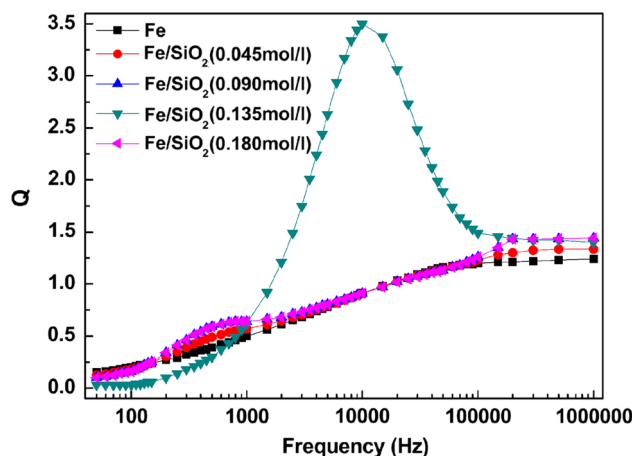
Figure 6 Frequency dependence of the quality factor for the raw Fe core and Fe/SiO$_2$ composite cores added different TEOS concentration.

Figure 6 illustrates the variation of Q with frequency for raw Fe core and Fe/SiO$_2$ composite core. The Q is a dimensionless parameter that describes the high-frequency properties of soft magnetic materials. Higher Q means lower energy loss rate. The Q can be obtained from the following formula:

$$Q = \frac{1}{W\mu_i} \qquad (3)$$

where W stands for the core loss and μ_i represents the initial permeability [33]. As can be seen, the Q is similar for all the samples at frequencies below 1 kHz and above 100 kHz, while the Q of Fe/SiO$_2$ composite core added TEOS concentration of 0.135 mol l^{-1} increases sharply at 1 kHz and exhibits the maximum value of 3.5 at the frequency of 10 kHz. It shows much higher Q than that of the other composite cores in the frequency ranges of 1–100 kHz. From formula (3) we know that the permeability and core loss greatly affect the variation tendency of Q.

The introduction of inorganic insulating layer between Fe particles provides many advantages such as high density, high strength, low core loss and high permeability for soft magnetic composites. Furthermore, it develops an intergranular insulation and confines the eddy current inside particles, which can increase the resistivity so as to decrease the eddy current loss, increase the Q and enhance the frequency stability of permeability. It is also believed that soft magnetic composites with intergranular insulation between ferromagnetic particles are indeed suitable for application in electromagnetic transition in the mid and high frequency, and

the as-prepared intergranular insulated Fe/SiO$_2$ composite core can obviously improve energy conversion efficiency and is benefited to energy-saving for electric–magnetic switching device.

Conclusions

The intergranular insulated Fe/SiO$_2$ soft magnetic composite cores with insulated layers of adjustable thickness were successfully prepared by the modified Stöber method combined with the spark plasma sintering. Most of the conductive Fe particles were coated by insulated SiO$_2$ using the modified Stöber method. In the spark plasma sintering, the high compact and intergranular insulated cores were obtained quickly. All of Fe/SiO$_2$ composite cores exhibited much higher electrical resistivity, lower core loss, better frequency stability of permeability and large higher quality factor than that of raw Fe core. By controlling the TEOS concentration, the microstructure and magnetic properties of the intergranular insulated Fe/SiO$_2$ composite cores could be readily adjusted. The intergranular insulated Fe/SiO$_2$ composite core added TEOS of 0.135 mol l^{-1} showed the highest electrical resistivity (8.53 μΩ m), lowest core loss ($P_{10 \text{ mT}/130 \text{ kHz}} = 284$ W kg^{-1}), best frequency stability of permeability and largest quality factor (3.5 at a frequency of 10 kHz). It is believed that the as-prepared intergranular insulated Fe/SiO$_2$ composite core can obviously improve energy conversion efficiency and is benefited to energy-saving for electric–magnetic switching device.

References

[1] Suetsuna T, Suenaga S, Harada K (2016) Bulk nanogranular composite of magnetic metal and insulating oxide matrix. Scr Mater 113:89–92

[2] Shokrollahi H, Janghorban K (2007) Soft magnetic composite materials (SMCs). J Mater Process Technol 189:1–12

[3] Jankowski B, Kapelski D, Ślusarek B et al (2015) Determination of power loss in Fe-based soft magnetic composites. Arch Metall Mater 60(2):1411–1415

[4] Liu C, Zhu J, Wang Y et al (2016) Design considerations of PM transverse flux machines with soft magnetic composite cores. IEEE Trans Appl Supercond 26(4):1–5

[5] Wang SX, Sun NX, Yamaguchi M et al (2000) Sandwich films: properties of a new soft magnetic material. Nature 407:150–151

[6] Lei G, Liu C, Guo Y et al (2016) Robust multidisciplinary design optimization of PM machines with soft magnetic composite cores for batch production. IEEE Trans Magn 52(3):1–4

[7] Gutfleisch O, Willard MA, Brück E et al (2011) Magnetic materials and devices for the 21st century: stronger, lighter, and more energy efficient. Adv Mater 23:821–842

[8] Oikonomou C, Hryha E, Nyborg L (2016) An XPS investigation on the thermal stability of the insulating surface layer of soft magnetic composite powder. Surf Interface Anal 48(7):445–450

[9] Bayramlı E, Gölgelioğlu Ö, Ertan HB (2005) Powder metal development for electrical motor applications. J Mater Process Technol 161(1):83–88

[10] Kollár P, Vojtek V, Birčáková Z et al (2014) Steinmetz law in iron–phenolformaldehyde resin soft magnetic composites. J Magn Magn Mater 353:65–70

[11] Dias MM, Mozetic HJ, Barboza JS et al (2013) Influence of resin type and content on electrical and magnetic properties of soft magnetic composites (SMCs). Powder Technol 237:213–220

[12] Wu S, Sun A, Zhai F et al (2012) Annealing effects on magnetic properties of silicone-coated iron-based soft magnetic composites. J Magn Magn Mater 324(5):818–822

[13] Peng Y, Nie J, Zhang W et al (2015) Preparation of soft magnetic composites for Fe particles coated with $(NiZn)Fe_2O_4$ via microwave treatment. J Magn Magn Mater 395:245–250

[14] Hemmati I, Hosseini HRM, Miraghaei S (2007) Effect of processing parameters on electrical, mechanical and magnetic properties of iron–resin soft magnetic composite. Powder Metall 50(1):86–90

[15] Uozumi G, Watanabe M, Nakayama R et al (2007) Properties of soft magnetic composite with evaporated MgO insulation coating for low iron loss. Mater Sci Forum 534:1361–1364

[16] Liu D, Wu C, Yan M (2015) Investigation on sol–gel Al_2O_3 and hybrid phosphate-alumina insulation coatings for FeSiAl soft magnetic composites. J Mater Sci 50(20):6559–6566. doi:10.1007/s10853-015-9189-4

[17] Zhong X, Liu Y, Li J et al (2012) Structure and magnetic properties of FeSiAl-based soft magnetic composite with AlN and Al_2O_3 insulating layer prepared by selective nitridation and oxidation. J Magn Magn Mater 324:2631–2636

[18] Kang Y, Huang Y, Yang R et al (2016) Synthesis and properties of core–shell structured $Fe(CO)_5/SiO_2$ composites. J Magn Magn Mater 399:149–154

[19] Kim YB, Jee KK, Choi GB (2008) Fe-based nanocrystalline alloy powder cores with excellent high frequency magnetic properties. J Appl Phys 103(7):07E704-1–07E704-3

[20] Kim TH, Jee KK, Kim YB et al (2010) High-frequency magnetic properties of soft magnetic cores based on nanocrystalline alloy powder prepared by thermal oxidation. J Magn Magn Mater 322(16):2423–2427

[21] Zhao G, Wu C, Yan M (2016) Enhanced magnetic properties of Fe soft magnetic composites by surface oxidation. J Magn Magn Mater 399:51–57

[22] Wu S, Sun A, Lu Z et al (2015) Magnetic properties of iron-based soft magnetic composites with SiO_2 coating obtained by reverse microemulsion method. J Magn Magn Mater 381:451–456

[23] Stöber W, Fink A, Bohn E (1968) Controlled growth of monodisperse silica spheres in the micron size range. J Colloid Interface Sci 26:62–69

[24] Zhu J, Wei S, Haldolaarachchige N et al (2011) Electromagnetic field shielding polyurethane nanocomposites reinforced with core–shell Fe–Silica nanoparticles. J Phys Chem C 115:15304–15310

[25] Xu H, Wang R, Wei D et al (2015) Crystallization kinetics and magnetic properties of FeSiCr amorphous alloy powder cores. J Magn Magn Mater 385:326–330

[26] Soohoo RF (1979) Magnetic thin film inductors for integrated circuit applications. IEEE Trans Magn 15:1803–1805

[27] Ni X, Zheng Z, Hu X et al (2010) Silica-coated iron nanocubes: preparation, characterization and application in microwave absorption. J Colloid Interface Sci 341(1):18–22

[28] Tie SL, Lee HC, Bae YS et al (2007) Monodisperse Fe_3O_4/$Fe@SiO_2$ core/shell nanoparticles with enhanced magnetic property. Colloids Surf A 293(1):278–285

[29] Pal R, Kundu D (2009) Sol–gel synthesis of porous and dense silica microspheres. J Non-Cryst Solids 355(1):76–78

[30] Li X, Makino A, Kato H et al (2011) $Fe_{76}Si_{9.6}B_{8.4}P_6$ glassy powder soft-magnetic cores with low core loss prepared by spark-plasma sintering. Mater Sci Eng B-Solid 176:1247–1250

[31] Lin GQ, Li ZW, Chen L et al (2006) Influence of demagnetizing field on the permeability of soft magnetic composites. J Magn Magn Mater 305:291–295

[32] Wu S, Sun A, Zhai F et al (2012) Annealing effects on magnetic properties of silicone-coated iron-based soft magnetic composites. J Magn Magn Mater 324:818–822

[33] Wang R, Liu J, Wang Z et al (2012) Crystallization kinetics and magnetic properties of $Fe_{63.5}Co_{10}Si_{13.5}B_9Cu_1Nb_3$ nanocrystalline powder cores. J Non-Cryst Solids 358:200–203